Available online at www.sciencedirect.com
SCIENCE DIRECT®
Biochimica et Biophysica Acta 1758 (2006) 764–771
BIOCHIMICA ET BIOPHYSICA ACTA
BBA
http://www.elsevier.com/locate/bba

Phase diagram of stigmasterol-dipalmitoylphosphatidylcholine mixtures dispersed in excess water

Ruiguang Wu [a], Lin Chen [a,b], Zhiwu Yu [a,*], Peter J. Quinn [b]

[a] *Key Laboratory of Bioorganic Phosphorous Chemistry and Chemical Biology (Ministry of Education), Department of Chemistry, Tsinghua University, Beijing 100084, PR China*
[b] *Department of Biochemistry, King's College London, 150 Stamford Street, London SE1 9NH, UK*

Received 21 January 2006; received in revised form 18 April 2006; accepted 19 April 2006
Available online 5 May 2006

Abstract

As a simple model of rafts in plant cells, the effect of stigmasterol, one of the predominant sterols in plant plasma membranes, on the phase behavior of dipalmitoylphosphatidylcholine (DPPC) multilayers has been studied by X-ray diffraction (XRD), differential scanning calorimetry (DSC), and freeze-fracture electron microscopy (FFEM) techniques. A partial phase diagram of the binary system has been constructed. Particularly, the stigmasterol concentrations of the "left endpoint" and "right endpoint" of the three-phase line have been determined using the newly developed linear and nonlinear fitting method. They are 6.2 and 23.7 mol%, respectively. Furthermore, the resemblance and difference of phase diagrams of DPPC/stigmasterol, DPPC/cholesterol, and DPPC/ergosterol have been compared and the efficiency of these sterols in promoting the formation of the liquid-ordered domains (rafts) have also been discussed.

Keywords: Stigmasterol; DPPC; Phase diagram; X-ray diffraction; DSC; Raft

1. Introduction

There is accumulating evidence supporting a model of mammalian plasma membrane in which domains rich in cholesterol and saturated lipids coexist with domains rich in unsaturated phospholipids [1–5]. The cholesterol-rich domain structures, namely rafts or detergent-resistant membrane fractions (DRMs), have been implicated in numerous cellular processes, including signal transduction, protein sorting, cellular entry by toxins and viruses, and viral budding [6–10]. As the major sterol present in mammalian cells, cholesterol has been regarded as a critical component of rafts in cells [2,3,5].

Not limited to animal cells, DRMs rich in sphingolipid/sterol have also been isolated from plant cells, where the dominant sterol is not cholesterol [11–13]. Particularly, stigmasterol has been identified as one of the predominant sterols in plant rafts such as in tobacco lipid rafts [12,14]. Because stigmasterol is among the major sterols in plant plasma membranes [15,16], its role in the formation of raft structures has become an interesting topic recently. In a study of lipid mixtures containing natural sterols and sphingolipids using fluorescence quenching and detergent insolubility, Xu et al. have shown that, like cholesterol, stigmasterol promoted the formation of tightly packed liquid-ordered domains containing DPPC or sphingomyelin. And both cholesterol and stigmasterol promoted the insolubility of these domains [17]. There have also been reports on the effects of stigmasterol and other plant sterols on the phase behavior of DPPC multibilayers investigated by DSC, XRD, resonance energy transfer, and detergent-induced solubilization techniques [18,19].

Phosphatidylcholines (PCs) are among the major phospholipids of plasma membranes [20]. Saturated PCs are known to have very similar physical properties to that of saturated-chain sphingolipids [21]. Thus, DPPC/sterol mixtures have been

Abbreviations: DPPC, dipalmitoylphosphatidylcholine; XRD, X-ray diffraction; DSC, differential scanning calorimetry; SAXS, small-angle X-ray scattering; WAXS, wide-angle X-ray scattering; FFEM, freeze-fracture electron microscopy; $L_{\beta'}$, lamellar-gel phase; $P_{\beta'}$, rippled gel phase; L_{α}, liquid–crystal phase; $L_{o\beta}$, liquid-ordered phase; T_p, the peak temperature of the sharp components of deconvoluted DSC curves; T_{end}, the endpoint temperature of the broad components of deconvoluted DSC curves

* Corresponding author. Tel.: +86 10 6279 2492; fax: +86 10 6277 1149.
E-mail address: yuzhw@tsinghua.edu.cn (Z.W. Yu).

0005-2736/$ - see front matter © 2006 Elsevier B.V. All rights reserved.
doi:10.1016/j.bbamem.2006.04.017

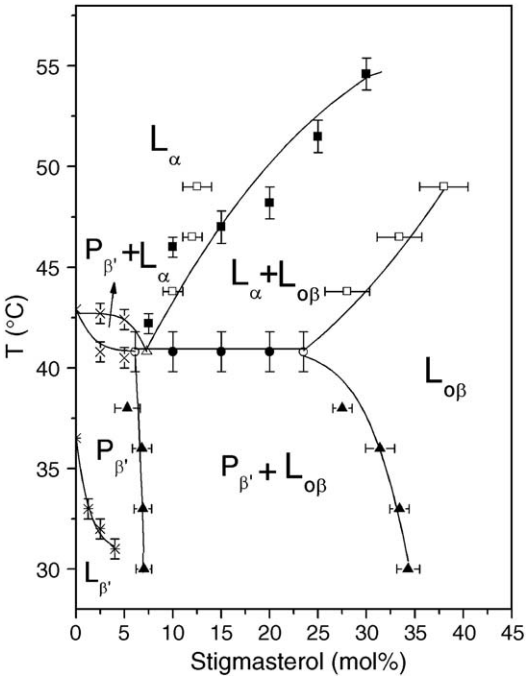

Fig. 1. Partial phase diagram of the stigmasterol/DPPC mixtures in excess water. ▲ and □, from XRD data; ●, from the peak temperature of the sharp component in Fig. 3; ■ and ×, from the onset or endpoint temperatures of the broad component in Fig. 3; ○, evaluated from DSC data; ✻, from the peak temperature of pretransition; △, estimated according to the trend of the upper boundaries of $P_{\beta'}+L_\alpha$ region and $L_\alpha+L_{o\beta}$ region. See text for details.

selected by many research groups as simple model systems of rafts. The partial phase diagram of DPPC/cholesterol has been constructed by Vist and Davis [22] and has received both experimental and theoretical support [23–25]. Recently, the partial phase diagram of DPPC/ergosterol (the predominant sterol in fungi) has been constructed by Hsueh et al. [26]. All these studies employed DSC and ^{2}H NMR techniques to determine the phase boundaries. Both these two diagrams contain three two-phase regions and a three-phase line, and three distinct phases have been identified: lamellar liquid–crystal (L_α) or liquid-disordered phase (L_d), lamellar-gel ($L_{\beta'}$) or solid-ordered phase (so), and liquid-ordered phase (L_o) [22,26]. No phase diagrams of stigmasterol-containing lipid mixtures has so far been published. The aim of this work is to study the effect of stigmasterol on the phase behavior of DPPC and to construct a partial phase diagram.

2. Materials and methods

2.1. Materials

1,2-Dipalmitoyl-*sn*-glycero-3-phosphocholine (DPPC) was purchased from Sigma Chemicals (St. Louis, MO, USA). Stigmasterol was from MP Biomedicals Inc. (95%, Aurora, OH, USA). They were used without further purification. DPPC/stigmasterol mixtures with designated mole ratios were dissolved in chloroform, dried under nitrogen, and then stored in vacuum overnight. The lipid films were hydrated with excess Tris–HCl buffers (50 mM Tris–HCl, 150 mM NaCl, 0.1 mM $CaCl_2$, pH 7.2) with repeated vortexing and heating to 60 °C and then stored at −20 °C at least for 24 h before experiments. The molar fraction of stigmasterol was 1.25%, 2.5%, 4%, 5%, 7.5%, 10%, 15%, 20%, 22.5%, 25%, 27.5%, 30%, respectively.

2.2. Experimental methods

2.2.1. X-ray diffraction (XRD) experiments

Real-time synchrotron X-ray diffraction experiments were performed at Station BL40B2 of Spring-8, Japan. The SAXS/WAXS data were recorded online with an image plate detector. The wavelength is 0.1 nm, and camera length was about 400 mm. A standard sample silver behenate was used for calibration. A Linkam thermal stage was used in temperature control. The temperature-scanning rate was 0.5 °C/min. Time for image exposure, data processing, and dumping was 330 s.

2.2.2. Differential scanning calorimetry

The calorimetry was performed by a Mettler-Toledo DSC821^e differential scanning calorimeter. Usually 20 μl of sample was used in each scanning experiment with the scan rate of 0.5 °C/min. In addition, a scanning rate of 5 °C/min has also been applied to detect the low enthalpic pretransition of DPPC multibilayers. Measurements were repeated at least three times to ensure reproducibility.

2.2.3. Freeze-fracture electron microscopy

Samples and tools used for sample manipulation were equilibrated at the desired temperature for at least 15 min. A small drop of the suspension was sandwiched between two copper plates and manually plunged into liquid nitrogen. The freeze-fracture procedure was carried out in a Balzers BAF 400D freeze-fracture apparatus. Fractured surfaces were shadowed with platinum/carbon. Platinum and carbon evaporation was done from 45 and 90° angle, respectively. Replicas were floated on a methanol–chloroform (1:3, v:v) solvents. Images were recorded with a FEI Tecnai 20 transmission electron microscope.

Deconvolution of the multicomponent XRD spectra and DSC curves was carried out using PeakFit software (Aisn Software Inc). The baseline was created by the two-point linear method and peak type was Gauss+Lorentz for all the

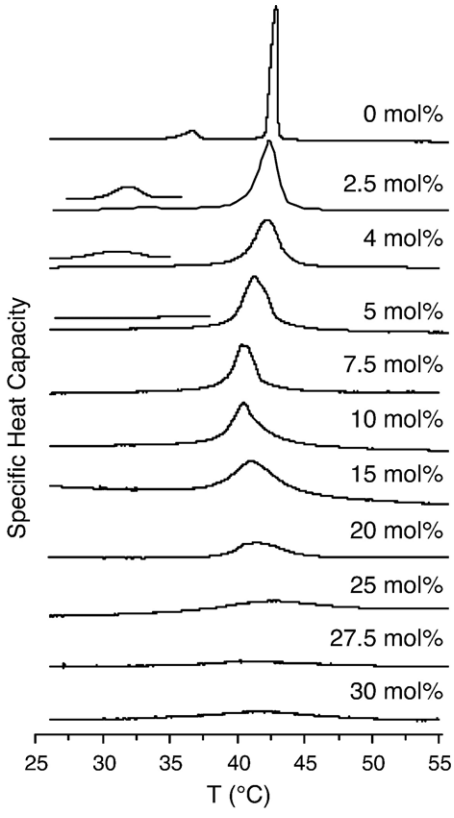

Fig. 2. DSC thermograms of stigmasterol/DPPC mixtures containing different molar percentage of stigmasterol. The scanning rate was 0.5 °C/min. Faster scanning rate (5 °C/min) was also employed in 2.5, 4, and 5 mol% stigmasterol to achieve larger differential signals.

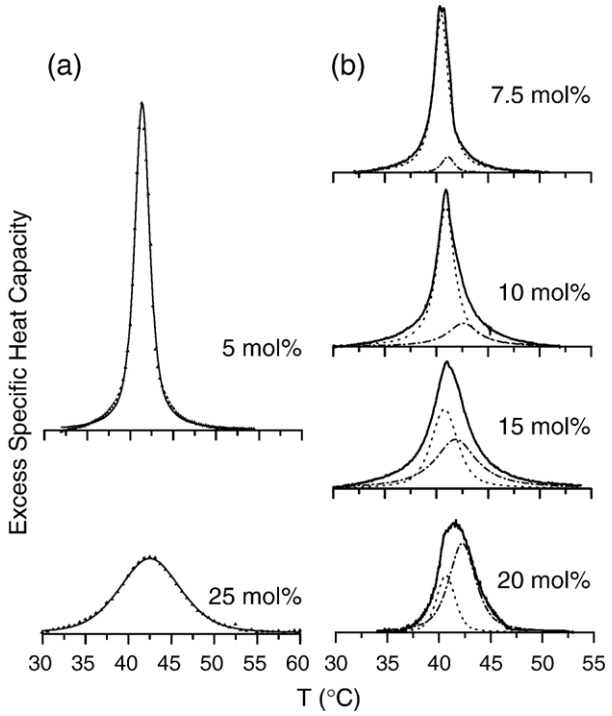

Fig. 3. Representative deconvoluted endotherms of the main transition of DPPC with different molar fractions of stigmasterol. Either one peak (a) or two peaks can be deconvoluted (b). Solid lines represent experimental curves; dotted and dash dotted lines, as well as triangles, represent the deconvoluted peaks, respectively.

deconvolution treatments. The liquid-ordered domains rich in sterol are designated as $L_{o\beta}$ phase in this work, following McElhaney and coworkers [27].

3. Results and discussion

A partial phase diagram of DPPC-stigmasterol, as shown in Fig. 1, has been established based on the experimental data of DSC, XRD, and FFEM. The boundaries of $L_{\beta'}/P_{\beta'}$, $P_{\beta'}/(P_{\beta'}+L_\alpha)$, and $(P_{\beta'}+L_\alpha)/L_\alpha$ were based on the pre- and main-transition of DSC results (stars and crosses); the three-phase line and the boundary of the $(L_\alpha+L_{o\beta})/L_\alpha$ were determined from the deconvolution results of DSC traces (solid squares); the boundary of the $L_{o\beta}/(L_\alpha+L_{o\beta})$ was determined from the fitting results of XRD data (open squares); the boundaries of $P_{\beta'}/(P_{\beta'}+L_{o\beta})$ and $(P_{\beta'}+L_{o\beta})/L_{o\beta}$ were determined from the fitting results of XRD data (solid triangles); and the ripple phase is identified by both FFEM and XRD techniques. Details are explained below.

3.1. Low stigmasterol region (0–5 mol%)

DSC thermograms of stigmasterol/DPPC mixtures recorded at a scan rate of 0.5°/min. are presented in Fig. 2. In the absence of stigmasterol, DPPC dispersions display a low enthalpic pretransition ($L_{\beta'}$ to $P_{\beta'}$) at 36.8 °C and a sharp main transition ($P_{\beta'}$ to L_α) at 42.9 °C, which are determined as the peak temperatures of the DSC curves following McMullen and McElhaney [27]. The phase transition temperatures are in good agreement with published data [28].

Similar phase behavior was recorded for dispersions containing less than 5 mol% of stigmasterol. First, the main phase transition endothermic peak becomes broadened in the presence of stigmasterol. Particularly, the transition temperature decreases with increasing concentration of the sterol. The start and end points of the peaks have been used to define the coexisting region of $P_{\beta'}$ and L_α phases.

Second, the pretransition was also investigated with fast scan rate of 5°/min at the stigmasterol molar percentage of 2.5, 4, and 5 mol%. The endothermic peaks are shown in Fig. 2 as insertions. Clearly, the pretransition temperature decreases with increasing concentration of sterol from 0 to 4 mol%. It is undetectable at higher than 5 mol% stigmasterol. This is in agreement with the report by Thompson and coworkers [18]. The $L_{\beta'}/P_{\beta'}$ boundary was simply evaluated by the peak temperature of the pretransition.

3.2. Determination of the three-phase coexistence line by calorimetry

Along with increasing stigmasterol, the peaks of main transitions become broadened, and an asymmetric feature appeared when the molar ratio is greater than 5%, indicating that the dispersions may consist of more than one phase. A recent study found that DPPC dispersions containing more than 5 mol% stigmasterol could be separated into sterol-poor and sterol-rich domains [19]. We have, therefore, tried to deconvolute these thermograms and found those containing 7.5 to 20 mol% stigmasterol could be well expressed by two components as depicted in Fig. 3. One is sharp, and the other is broad. The sharp peaks all have almost the same peak temperature, 40.8 °C, with an error of ±0.3 °C. The endpoint temperature of the broad coponent increases gradually with increasing concentration of the sterol. These data are summarized in Table 1. By contrast, the thermograms containing less than 5% or more than 25% stigmasterol are symmetric and are believed to originate from a single-phase transition.

Accordingly, the following conclusion can be made: (1) the temperature, where $P_{\beta'}+L_{o\beta}+L_\alpha$ three-phase coexists, is about 40.8 °C; (2) the minimum sterol concentration of the three-phase line, or the "left endpoint" (ϕ), is between 5 and 7.5 mol%; (3) the maximum sterol concentration of the three-phase line, or the "right endpoint "(θ), is between 20 and 25 mol%.

We now evaluate the precise values of ϕ and θ. We assume that, for the two deconvoluted thermal events shown in Fig. 3(b), the sharp component is contributed by the phase transition enthalpy from $P_{\beta'}$ to L_α phase containing ϕ mol% stigmasterol, and the broad component represents the phase transition enthalpy from $L_{o\beta}$ to L_α phase containing θ mol% stigmasterol. A_p^α

Table 1
The peak temperature of the sharp component (T_p) and the endpoint temperature of the broad component (T_{end}) in Fig. 3

Sterol (mol%)	T_p (°C)	T_{end} (°C)
7.5	40.4±0.3	42.2±0.4
10	40.8±0.3	46.3±0.4
15	41.0±0.3	47.2±0.4
20	41.0±0.3	48.1±0.4

Table 2
The fitted values of θ and h at some given value of ϕ

ϕ	θ	h	R^2
3	18	4.2	0.81
4	19	3.1	0.84
5	20	2.1	0.90
5.5	21	1.6	0.94
6	23	1.1	0.99
6.5	25	0.7	0.95
6.7	20	0.9	0.34

and A_l^{α} are defined as the areas of the two components, n_p and n_l the moles of molecules of each phase involved, $\Delta_p^{\alpha}H_m$ and $\Delta_l^{\alpha}H_m$ the phase transition enthalpies per mole of DPPC from $P_{\beta'}$ to L_{α} and from $L_{o\beta}$ to L_{α}, respectively. Then the following equation can be given:

$$A_p^{\alpha}=n_p\times(100-\phi)\times\Delta_p^{\alpha}H_m \quad (1)$$

$$A_l^{\alpha}=n_l\times(100-\theta)\times\Delta_l^{\alpha}H_m \quad (2)$$

We further define $\lambda=\frac{A_p^{\alpha}}{A_l^{\alpha}}$ and $h=\frac{\Delta_p^{\alpha}H_m}{\Delta_l^{\alpha}H_m}$. The former can be determined by deconvolved endothermic peaks. Then for a given sterol molar percentage x in a DPPC/sterol mixture, following equation can be obtained according to the lever rule,

$$\lambda=\frac{(\theta-x)}{(x-\phi)}\times\frac{(100-\phi)}{(100-\theta)}\times h \quad (3)$$

which can be rearranged into the following form,

$$x=\frac{\lambda(\phi-x)}{(100-\phi)}\times\frac{(100-\theta)}{h}+\theta \quad (4)$$

In Eq. (4), h, ϕ, and θ are unknown parameters, but they are constants. By assigning a value to ϕ, the values of h and θ can be obtained from linear fitting when plotting x as a function of $\lambda(\phi-x)/(100-\phi)$. The fitting results are summarized in Table 2. The best set of the fitting is selected according to the correlation coefficient R^2, which gives ϕ=6 and θ=23. Taking these values and h=1.1 as initializing parameters, the nonlinear least squares fitter of Microcal Origin can further refine the parameters as ϕ=6.2 and θ=23.7. They fall precisely into the range predicted before.

The $(L_{\alpha}+L_{o\beta})/L_{\alpha}$ boundary was determined from the endpoint of the broad deconvolution results at $7.5\% \le x \le 20\%$ and the endpoint of the raw DSC traces at $x \ge 25\%$ (solid squares). According to the trend of the upper boundaries of $P_{\beta'}+L_{\alpha}$ and $L_{\alpha}+L_{o\beta}$, the eutectic point or triple point is expected to be around 7 mol% stigmasterol (open triangle).

3.3. Determination of phase boundaries $P_{\beta'}/(P_{\beta'}+Lo_{\beta})$ and $(P_{\beta'}+Lo_{\beta})/Lo_{\beta}$ by XRD

X-ray diffraction patterns were recorded over the temperature range 30 °C to 63 °C at intervals of 2.75 °C at a heating rate of 0.5°/min. In the absence of stigmasterol, a DPPC dispersion shows two phase transitions in the temperature range, namely from lamellar-gel ($L_{\beta'}$) to ripple ($P_{\beta'}$) and then to liquid–crystal phase (L_{α}). This is in agreement with the DSC results. At least five orders of diffraction have been recorded in the small-angle region for each of the mixed lipid dispersions. The reciprocal spacings of these diffractions show a ratio of 1:2:3:4:5, characterizing all the structures as lamellar.

Representative small-angle (SAXS) and wide-angle X-ray scattering (WAXS) patterns for a dispersion of DPPC containing 10 mol% stigmasterol are presented in Fig. 4. Only the first two orders in the small-angle region are shown to clarify the presentation. As can be seen, the spacing of the first-order SAXS pattern decreases abruptly from about 8.0 nm at 38.3 °C to about 6.9 nm at 43.8 °C, indicating a main phase transition of DPPC dispersion from gel phase to the L_{α} phase. The transformation of a sharp diffraction at 0.42 nm (38.3 °C) to a broad scattering at 0.45 nm (43.8 °C) in the WAXS region also indicates the main phase transition.

An asymmetric feature in the diffraction maxima can also be seen in Fig. 4, especially for the small angle diffraction patterns. This suggests that the peaks can be deconvolved into two peaks just as demonstrated for the DSC thermal peaks. As the first-order of the SAXS spectra overlaps extensively, the second-order of the SAXS profiles has been selected to perform the analyses in this work.

Shown in Fig. 5 is an example of the deconvolution process, which shows the SAXS peak from the DPPC dispersion containing 10 mol% stigmasterol at 38.3 °C can be deconvolved into a sharp and a broad peak. By comparison with the phase

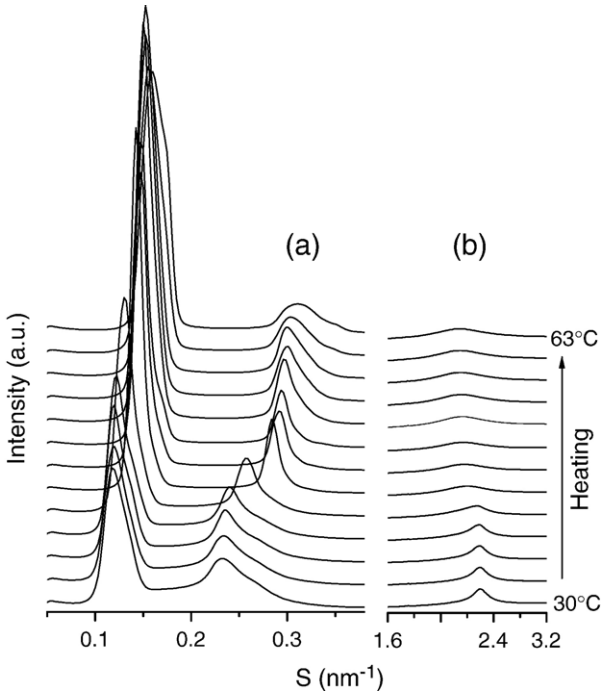

Fig. 4. Small-angle (a) and wide-angle (b) X-ray diffraction patterns recorded from a stigmasterol/DPPC binary mixture (containing 10 mol% stigmasterol) as a function of reciprocal spacing during a heating scan at 0.5 °C/min. The temperature interval was 2.75 °C.

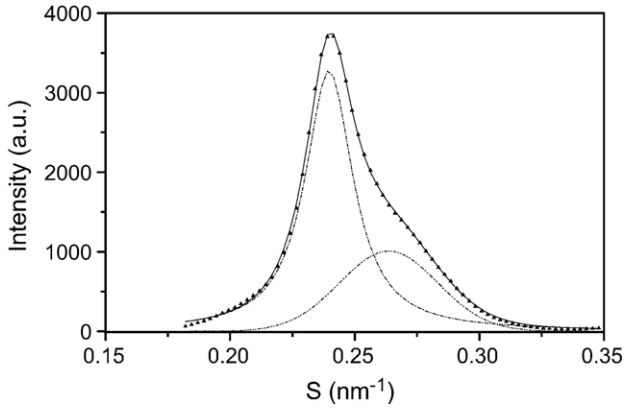

Fig. 5. Representative deconvolution of the second-order SAXS of a stigmasterol/DPPC mixture containing 10 mol% stigmasterol at 38.3 °C. Triangles are experimental data, solid line represents the overall fitting spectrum.

diagrams of cholesterol-DPPC [22] and ergosterol-DPPC [26] binary systems, it can be assumed that the two components are sterol-poor and sterol-rich domains, respectively. The former is a gel phase, which has been characterized as a ripple phase (see next section). The latter is a $L_{o\beta}$ phase.

It is reasonable to assume that the integrated areas of the two peaks, S_1 and S_2, are in direct proportion to the amount of the respective lamellar phase, with coefficients f_1 and f_2. At a given temperature, the two domains should have fixed compositions, say ϕ and θ mol% of stigmasterol. For a lipid mixture containing x mol% stigmasterol, according to the lever rule, the following equation can be obtained:

$$S_1 f_1 (x-\phi) = S_2 f_2 (\theta - x) \quad (5)$$

By further defining $\frac{S_1}{S_2}=\lambda$, $\frac{f_1}{f_2}=f$ the above equation can be rearranged into the following form:

$$x = f[\lambda(\phi - x)] + \theta \quad (6)$$

In Eq. (6), f, ϕ, and θ are unknown parameters, but they are constants at a given temperature. The value of x is a known parameter and λ can be obtained by integrated area of deconvoluted peaks. By assigning a value to ϕ, f, and θ can be obtained from linear least square fitting when plotting x as a function of $\lambda(\phi - x)$. The values of λ of mixtures containing more than 5 mol% sterol at 33 °C are summarized in Table 3. As shown in the table, the values of λ decrease with increasing x. This agrees with the lever rule: as x increases at a given temperature, the quantity ratio of the gel phase to $L_{o\beta}$ phase decreases, thus λ decreases. The fitting values of θ and f at 33 °C are summarized in Table 4 when given different values of ϕ. The criteria in choosing the value of ϕ are the maximum correlation coefficient R^2. Thus, the optimum parameters are ϕ=6, θ=31. The correlation coefficient R^2 will decrease when ϕ is lower or higher than 6. Taking these values and f=2.3 as initializing parameters, the nonlinear least squares fitter of Microcal Origin can further refine the parameters as ϕ=6.8 and θ=32.1. That is to say, the stigmasterol concentrations in the sterol-poor domain and the sterol-rich domain are 6.8% and 32.1%, respectively.

Table 3
Peak areas and their ratio λ at 33 °C

x (%)	S_1	S_2	λ
10	131.2	55.1	2.4
15	61.4	87.8	0.7
20	59.5	152.0	0.4
25	15.2	149.6	0.1
30	7.2	137.9	0.05

Table 4
The fitted values of θ and f when given different values of ϕ at 33 °C

ϕ	θ	f	R^2
0	27.5	0.8	0.86
1	27.7	0.9	0.87
2	28.1	1.0	0.88
3	28.5	1.2	0.90
4	29.1	1.4	0.92
5	29.9	1.8	0.94
6	31.0	2.3	0.96
7	32.4	3.0	0.95
8	33.2	3.9	0.82
9	28.4	3.1	0.33

Parameters of ϕ and θ at other temperatures can be derived in the same way. They are summarized in Table 5. The results below 40 °C have been used to construct the boundaries of $P_{\beta'}/(P_{\beta'}+L_{o\beta})$ and $(P_{\beta'}+L_{o\beta})/L_{o\beta}$ (solid triangles in Fig. 1.); while data at 44° and 47 °C were used to establish the boundary of $L_{o\beta}/(L_\alpha+L_{o\beta})$ (open squares in Fig. 1).

3.4. Identification of the ripple phase

We will provide evidence that the sterol-poor phase at temperatures below 40 °C is rippled gel phase ($P_{\beta'}$) but not $L_{\beta'}$ phase. Although Fig. 2 shows that the pretransition cannot be detected by adding more than 5 mol% stigmasterol, this does not necessarily mean that the $P_{\beta'}$ phase does not exist when $x>5$%. It has been reported in DSC studies that the pretransition was suppressed by adding more than 6 mol% cholesterol to DPPC or DMPC [22,29], but the ripple phase structure remains even at 16 mol% [30] or 15 mol% [31] cholesterol content from the experiments of freeze-fracture electron microscopy. Recently, Hatta proposed a schematic phase diagram of PCs/cholesterol mixtures based on DSC and XRD experiments, suggesting that

Table 5
The fitted values of θ and ϕ at different temperatures

T (°C)	ϕ	θ
30	7.0±0.5	34.3±1.2
33	6.8±0.6	32.1±1.0
36	6.8±1.0	31.4±1.5
38	5.5±1.3	28.5±1.0
44	10.0±1.0	28.0±2.5
47	12.0±1.0	33.4±2.5
49	12.5±1.4	38.0±2.7

the ripple phase exists in the whole region where sterol-poor and sterol-rich domains coexist under the temperature of the three-phase line [32].

The XRD features of $P_{\beta'}$ phase are significantly different from that of $L_{\beta'}$ phase. In the present study, as shown in Fig. 6, the diffraction patterns of the SAXS (a) and WAXS (b) spectra of pure DPPC at 30 °C and 38 °C represent the characteristics of the $L_{\beta'}$ phase and the $P_{\beta'}$ phase, respectively. Compared with the first- and second-order of the SAXS diffraction patterns of $L_{\beta'}$ phase, the diffraction intensity of $P_{\beta'}$ phase becomes lower and the diffraction peak tends to be more diffused. By contrast with the WAXS pattern of $L_{\beta'}$ phase, the intensity of diffraction of $P_{\beta'}$ phase becomes lower and the diffraction peak tends to be more symmetric [33]. Because the gel phase (sterol-poor domains) is predominant at ~5 to 10 mol% sterol according to the phase diagram, the X-ray scattering pattern signifies a gel phase in this concentration range. As seen in Fig. 6(a), the diffuse appearance of the first- and second-order peaks of the SAXS pattern as well as the symmetric WAXS pattern at x=5% and x=10% strongly suggest that the gel phase (sterol-poor domains) is a ripple phase ($P_{\beta'}$). At higher stigmasterol concentrations, the diffraction patterns in the SAXS region do not show the characteristics of ripple phase. This may be due to the overlapping of $P_{\beta'}$ with the dominant $L_{o\beta}$ phase. The symmetric WAXS pattern in this region, however, suggests that the phase is not a typical $L_{\beta'}$ phase.

The periodicity of the ripple phase of DPPC in the absence of stigmasterol was determined to be 13.2 nm (S=0.076 nm^{-1}) by the SAXS reflection appearing in the lower angle to the first-order of the lamellar repeat, indicated by an arrow (Fig. 6(c)). This was in good agreement with the result of Bóta and coworkers [34]. The periodicity of ripple phase at other concentrations with ≥5 mol% stigmasterol could not be determined unambiguously by X-ray diffraction method due to low signal/noise ratio. This is in line with the recent report by Matuoka and coworkers where a codispersion of DMPC and cholesterol was investigated [35].

To identify the existence of the rippled gel phase further, electron micrographs of freeze-fracture replicas prepared from the codispersions of DPPC with 15 mol% stigmasterol thermally quenched from 30 °C were examined. The representative image in Fig. 6(d) shows the well-characterized rippled freeze-fracture pattern of the $P_{\beta'}$ phase (see [36] for review). The ripple periodicity was estimated as 35–45 nm, much larger than that of pure DPPC. This agrees with the conclusion that ripple periodicity of DPPC containing different cholesterol concentrations increases with increasing sterol concentrations [31,35].

Phase diagrams of DPPC/sterol binary dispersions are very useful in characterizing the interactions between the particular

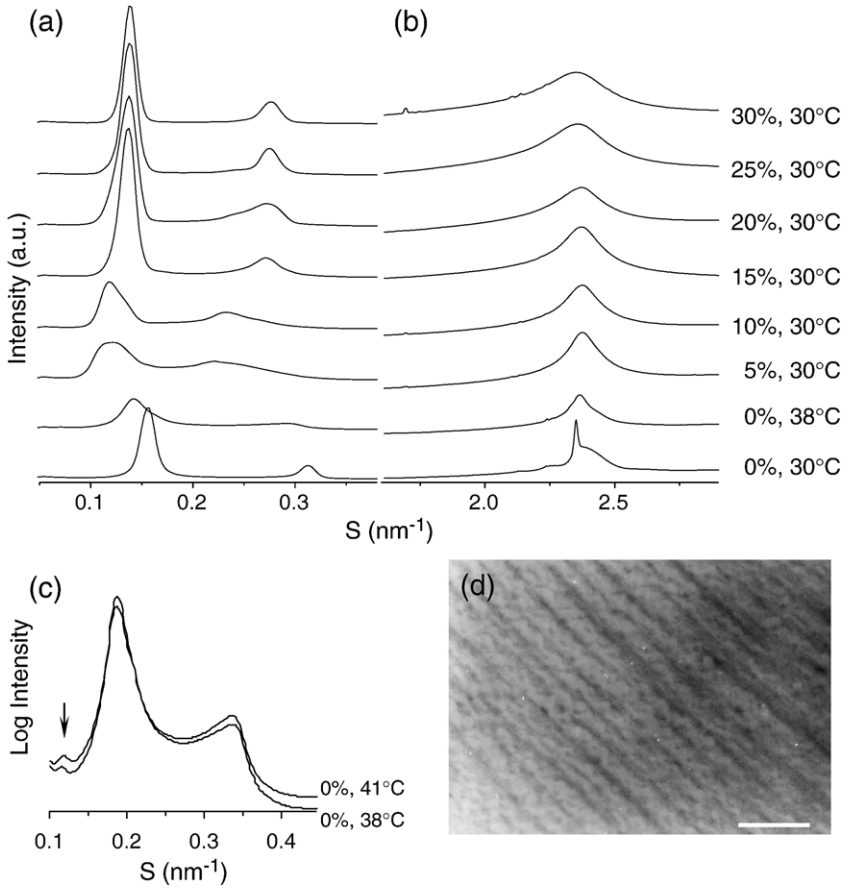

Fig. 6. Small-angle (a) and wide-angle (b) X-ray diffraction patterns recorded from DPPC-stigmasterol codispersions. The WAXD intensities were enlarged to show the patterns more clearly. (c) Logarithm plot of the SAXD profiles of DPPC dispersed in water at two indicated temperatures, emphasizing the minor bands from the ripple phase. The molar percentage of stigmasterol and the scanning temperature had been labeled on the right of the corresponding curves. (d) FFEM image of a DPPC codispersion containing 15 mol% stigmasterol. The scale bar corresponds to 100 nm.

lipid species. Together with present work, three DPPC/sterol binary systems have been examined. It is thus worthwhile to compare the phase diagram presented in this report and that of DPPC/cholesterol [22] and DPPC/ergosterol [26]. First, all three-phase diagrams contain a three-phase line and three two-phase regions. In the case of systems containing cholesterol and ergosterol, lamellar-gel phase and ripple phase were combined as a "*gel* phase" or solid-ordered phase. Hatta's recent work, however, distinguished the ripple phase from normal lamellar-gel phase [32]. Second, all the boundaries of gel/(gel+$L_{o\beta}$) in the three diagrams are practically vertical. But the (gel+$L_{o\beta}$)/$L_{o\beta}$ boundaries of DPPC/ergosterol and DPPC/stigmasterol slope from 25 mol% and 27 mol% near 38 °C to 32 mol% and 34 mol% near 30 °C, respectively. In the case of DPPC/cholesterol mixtures, the boundary is observed to be nearly vertical around 23 mol%. This means that cholesterol has higher efficiency than stigmasterol or ergosterol in forming liquid-ordered phase. It should be noted that the sequential order of these sterols in promoting the formation of liquid-ordered phases are not necessarily the order in which they promote the formation of rafts in vivo. Any difference in sterol/sphingolipid/phospholipid ratios among mammalian cell, fungal cell, and plant cell could significantly influence the lipid raft formation in vivo [13]. Nevertheless, the present study may help to understand the principles that underlie the formation of rafts in vivo. Third, the temperatures of three-phase lines are 40.8°, 39.5°, and 37 °C for stigmasterol, ergosterol, and cholesterol, respectively, in the phase diagrams. In the cases of ergosterol and cholesterol, d_{31}-DPPC and d_{62}-DPPC were used respectively. Klump et al. previously reported that the main transition temperature of d_{31}-DPPC and d_{62}-DPPC were 2.3 °C and 4.1 °C lower than undeuterated DPPC [37]. Taking this difference into account, the temperatures of the three-phase lines will be 40.8°, 41.8°, and 41.1 °C for stigmasterol/DPPC, ergosterol/DPPC, and cholesterol/DPPC, respectively. There is no significant difference between these values.

In conclusion, a partial phase diagram of DPPC and stigmasterol binary system has been constructed by the methods of DSC, X-ray diffraction, and FFEM. Particularly, the stigmasterol concentrations of the "left endpoint" and "right endpoint" of the three-phase line have been determined using the newly developed linear and nonlinear fitting method. They are 6.2 and 23.7 mol%, respectively. Furthermore, this study suggests that the efficiency of stigmasterol to promote the formation of liquid-ordered domains (rafts) containing DPPC is lower than that of cholesterol.

Acknowledgements

This work was supported by grants from the Natural Science Foundation of China (NSFC: 20373032, 20505012) and a joint program between NSFC and the Royal Society (UK). Assistance of Dr. Inoue from SPring-8 (Japan) is gratefully acknowledged.

References

[1] D.A. Brown, J.K. Rose, Sorting of GPI-anchored proteins to glycolipid enriched membrane subdomains during transport to the apical cell surface, Cell 68 (1992) 533–544.
[2] D.A. Brown, E. London, Functions of lipid rafts in biological membranes, Annu. Rev. Cell Dev. Biol. 14 (1998) 111–136.
[3] D.A. Brown, E. London, Structure and origin of ordered lipid domains in biological membranes, J. Membr. Biol. 164 (1998) 103–114.
[4] D.A. Brown, E. London, Structure and function of sphingolipid- and cholesterol-rich membrane rafts, J. Biol. Chem. 275 (2000) 17221–17224.
[5] K. Simons, D. Toomre, Lipid rafts and signal transduction, Nat. Rev., Mol. Cell Biol. 1 (2000) 31–39.
[6] T.Y. Wang, R. Leventis, J.R. Silvius, Artificially lipid-anchored proteins can elicit clustering-induced intracellular signaling events in Jurkat T-lymphocytes independent of lipid raft association, J. Biol. Chem. 280 (2005) 22839–22846.
[7] A. Vidal, T.J. McIntosh, Transbilayer peptide sorting between raft and nonraft bilayers: comparisons of detergent extraction and confocal microscopy, Biophys. J. 89 (2005) 1102–1108.
[8] I. Rousso, M.B. Mixon, B.K. Chen, P.S. Kim, Palmitoylation of the HIV-1 envelope glycoprotein is critical for viral infectivity, Proc. Natl. Acad. Sci. U.S.A. 97 (2000) 13523–13525.
[9] S. Mukherjee, T.T. Soe, F.R. Maxfield, Endocytic sorting of lipid analogues differing solely in the chemistry of their hydrophobic tails, J. Cell Biol. 144 (1999) 1271–1284.
[10] A.A. Wolf, M.G. Jobling, S. Wimer-Mackin, M. Ferguson-Maltzman, J.L. Madara, R.K. Holmes, W.I. Lencer, Ganglioside structure dictates signal transduction by cholera toxin and association with caveolae-like membrane domains in polarized epithelia, J. Cell Biol. 144 (1998) 917–927.
[11] T. Peskan, M. Westermann, R. Oelmuller, Identification of low-density Triton X-100 insoluble plasma membrane microdomains in higher plants, Eur. J. Biochem. 267 (2000) 6989–6995.
[12] S. Mongrand, J. Morel, J. Laroche, S. Claverol, J.P. Carde, et al., Lipid rafts in higher plant cells: purification and characterization of Triton X-100-insoluble microdomains from tobacco plasma membrane, J. Biol. Chem. 279 (2004) 36277–36286.
[13] G.H.H. Borner, D.J. Sherrier, T. Weimar, L.V. Michaelson, N.D. Hawkins, et al., Analysis of detergent-resistant membranes in *Arabidopsis*. Evidence for plasma membrane lipid rafts, Plant Physiol. 137 (2005) 104–116.
[14] S.W. Martin, B.J. Glover, J.M. Davies, Lipid microdomains-plant membranes get organized, Trends Plant Sci. 10 (2005) 263–265.
[15] R.A. Demel, B.D. Kruyff, The function of sterols in membranes, Biochim. Biophys. Acta 457 (1976) 109–132.
[16] B.D. Mckersie, J.R. Lepock, J. Kruuv, J.E. Thompson, The effects of cotyledon senescence on the composition and physical properties of membrane lipid, Biochim. Biophys. Acta 508 (1978) 197–212.
[17] X.L. Xu, R. Bittman, G. Duportail, D. Heissler, C. Vilcheze, E. London, Effect of the structure of natural sterols and sphingolipids on the formation of ordered sphingolipid/sterol domains (rafts), J. Biol. Chem. 276 (2001) 33540–33546.
[18] B.D. McKersie, J.E. Thompson, Influence of plant sterols on the phase properties of phospholipid bilayers, Plant Physiol. 63 (1979) 802–805.
[19] K.K. Halling, J.P. Slotte, Membrane properties of plant sterols in phospholipid bilayers as determined by differential scanning calorimetry, resonance energy transfer and detergent-induced solubilization, Biochim. Biophys. Acta 1664 (2004) 161–171.
[20] S. Karmakar, V.A. Raghunathan, Structure of phospholipid–cholesterol membranes: an X-ray diffraction study, Phys. Rev., E Stat. Phys. Plasmas Fluids Relat. Interdiscip. Topics 71 (2005) 061924.
[21] H. Ohvo-Rekilä, B. Ramstedt, P. Leppimäki, J.P. Slotte, Cholesterol interactions with phospholipids in membranes, Prog. Lipid Res. 41 (2002) 66–97.
[22] M.R. Vist, J.H. Davis, Phase equilibria of cholesterol/dipalmitoylphosphatidylcholine mixtures: ^{2}H nuclear magnetic resonance and differential scanning calorimetry, Biochemistry 29 (1990) 451–464.
[23] F.M. Linseisen, J.L. Thewalt, M. Bloom, T.M. Bayerl, Deuterium-NMR and DSC study of SEPC-cholesterol mixtures, Chem. Phys. Lipids 65 (1993) 141–149.
[24] T. Murtola, E. Falck, M. Patra, M. Karttunen, I. Vattulainen, Coarse-grained model for phospholipid/cholesterol bilayer, J. Chem. Phys. 121 (2004) 9156–9165.
[25] J.H. Ipsen, G. Karlstroem, O.G. Mouritsen, H. Wennerstroem, M.J. Zuckermann, Phase equilibria in the phosphatidylcholine-cholesterol system, Biochim. Biophys. Acta 905 (1987) 162–172.

[26] Y.W. Hsueh, K. Gilbert, C. Trandum, M. Zuchermann, J. Thewalt, The effect of ergosterol on dipalmitoylphosphatidylcholine bilayers: a deuterium NMR and calorimetric study, Biophys. J. 88 (2005) 1799–1808.
[27] T.P.W. McMullen, R.N. McElhaney, New aspects of the interaction of cholesterol with dipalmitoylphosphatidylcholine bilayers as revealed by high-sensitivity differential scanning calorimetry, Biochim. Biophys. Acta 1234 (1995) 90–98.
[28] G.C. Goodwin, K. Hammond, I. Lyle, M.N. Jones, Lectin-mediated agglutination of liposomes containing glycophorin. Effects of acyl chain length, Biochim. Biophys. Acta 689 (1982) 80–88.
[29] T.P.W. McMullen, A.H. Lewis, R.N. McElhaney, Differential scanning calorimetric study of the effect of cholesterol on the thermotropic phase behavior of a homologous series of linear saturated phosphatidylcholines, Biochemistry 32 (1993) 516–522.
[30] B.R. Copeland, H.M. McConnell, The ripple structure in bilayer membranes of phosphatidylcholine and binary mixtures of phosphatidylcholines and cholesterol, Biochim. Biophys. Acta 599 (1980) 95–109.
[31] A. Hicks, M. Dinda, M.A. Singer, The ripple phase of phosphatidylcholines: effect of chain length and cholesterol, Biochim. Biophys. Acta 903 (1987) 177–185.
[32] I. Hatta, Temperature scanning X-ray diffraction at phase transitions of biologically related lipid assemblies, special attention to cholesterol-rich state, J. Therm. Anal. Calorim. 82 (2005) 189–192.
[33] Z.W. Yu, P.J. Quinn, Phase stability of phosphatidylcholines in dimethylsulfoxide solutions, Biophys. J. 69 (1995) 1456–1463.
[34] A. Bóta, T. Drucker, M. Kriechbaum, Z. Pálfia, G. Réz, Layer formations of dipalmitoylphosphatidylcholine liposomes in the pretransition range, Langmuir 15 (1999) 3101–3108.
[35] S. Matuoka, S. Kato, I. Hatta, Temperature change of the ripple structure in fully hydrated dimyristoylphosphatidylcholine/cholesterol multibilayers, Biophys. J. 67 (1994) 728–736.
[36] H.W. Meyer, W. Richter, Freeze-fracture studies on lipids and membranes, Micron 32 (2001) 615–644.
[37] H.H. Klump, B.P. Gaber, W.L. Peticolas, P. Yager, Thermodynamic properties of mixtures of deuterated and undeuterated dipalmitoylphosphatidylcholines (differential scanning calorimetry/lipid bilayers/membranes), Thermochim. Acta 48 (1981) 361–366.